Supplementary Material

Supplementary Figure S1

The Figure S1 shows the electric field distribution and surface current at the resonant frequencies of dip1 (0.680 THz) and dip 2 (1.627 THz), respectively. It can be observed in Figures S1 A and C that the electric energy is localized at the three gaps in the ring and the surface currents form a loop in each sector, respectively, indicating that the dip 1 originates from inductor-capacitor (LC) oscillation. In addition, the Figures S1 B and D show that the electric energy is localized at the left and right gaps of the ring and the surface currents flow from the left to right, forming signal enhancement due to the electric dipole oscillator.

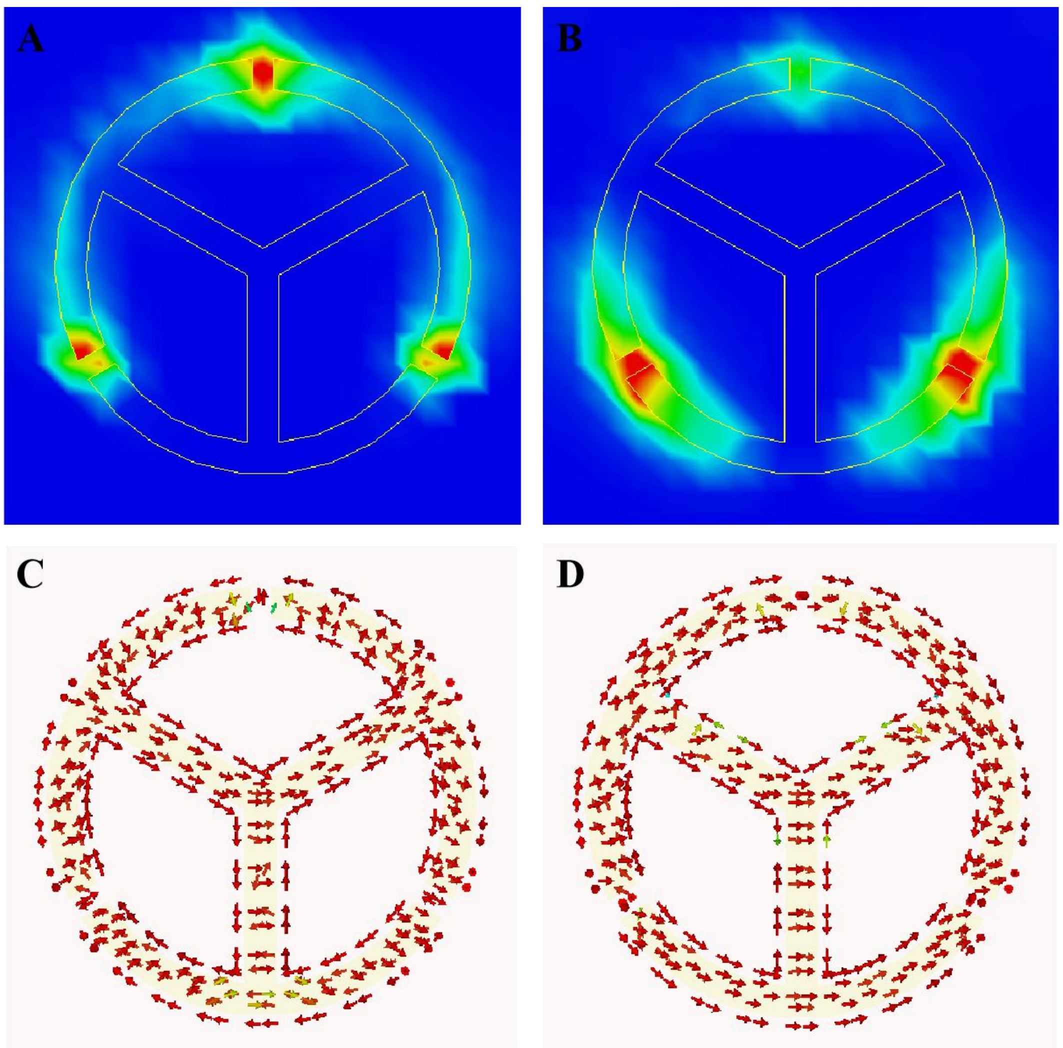

Figure S1 | The electric field distribution and surface current at the resonant frequencies of dip1 (0.680 THz) (A, C) and dip 2 (1.627 THz) (B, D), respectively.

Supplementary Figure S2

In order to further explore the influence of the opening numbers in the MM structure on the sensing performance, we additionally designed single split ring (SSR) and double split ring (DSR) MM biosensors. The geometric parameters of our proposed SSR and DSR MM biosensor are shown in the **Figure S2A**. The simulated transmission spectra of the SSR, DSR and TSR MM sensors are shown in **Figure S2B**. It can be observed that the resonance frequency of dip1 appears blue-shifted as the number of openings increases, which is the result of enhancement of the equivalent capacitance. It can also be noted that the FWHM of the resonance peak is gradually increasing, which can be attributed to the superimposition of the resonance peak. **Figure S2C** exhibits the sensitivity of the three meta-sensor under various refractive index of the analyte when the thickness is set to 4 μm. It can be seen that the proposed TSR biosensor has higher sensitivity compared to SSR and DSR biosensor. The theoretical sensitivity of the three MM biosensors is evaluated to 36.7, 41.4, and 48.9 GHz/RIU, respectively. Hence, our results effectively prove that the increase in the number of gaps can significantly improve the sensing performance.

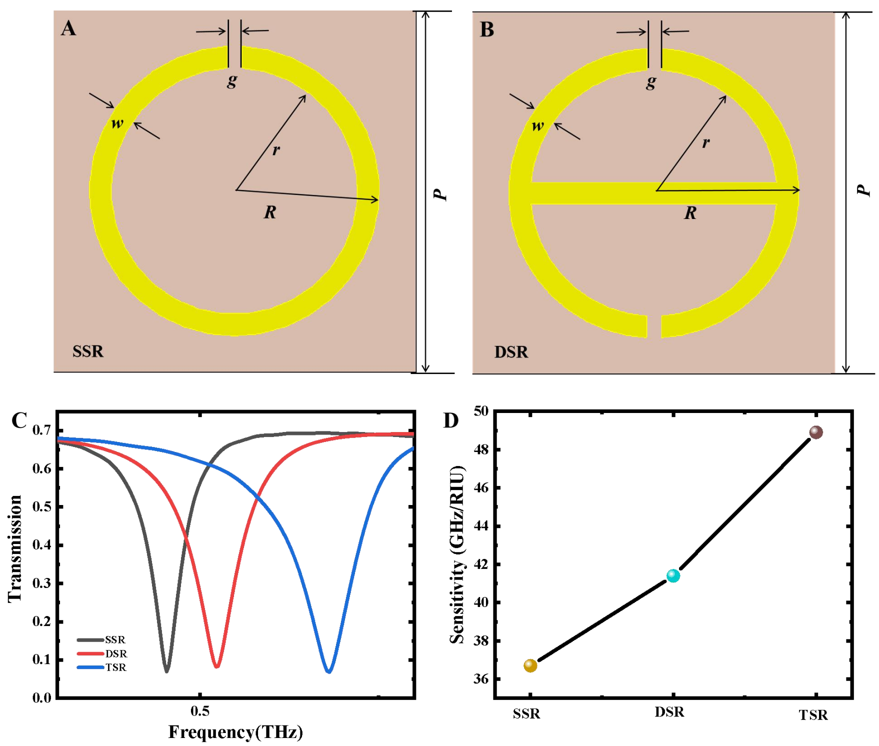

Figure S2 | (A)The geometric parameters of SSR and DSR meta-sensors.The simulated transmission spectra (B) and sensitivity (C) of the SSR, DSR and TSR MM sensors, respectively.

Supplementary Figure S3

The corresponding four cases with different quantities located in different position were discussed in the Supplementary **Figure S3**. It can be seen that the frequency shifts in the cases of III and IV with more analytes are hardly observable, while a significant red shift in the case of II with fewer analytes is presented. In addition, the theoretical sensitivity for the case of II with fewer analytes has higher sensitivity compared to the cases of III and IV with more analytes (Figure S3C). Through the above simulation, we proved that the similar results can be obtained when the target samples with different quantities located in different position due to the effective area of near-field coupling is at the three gaps.

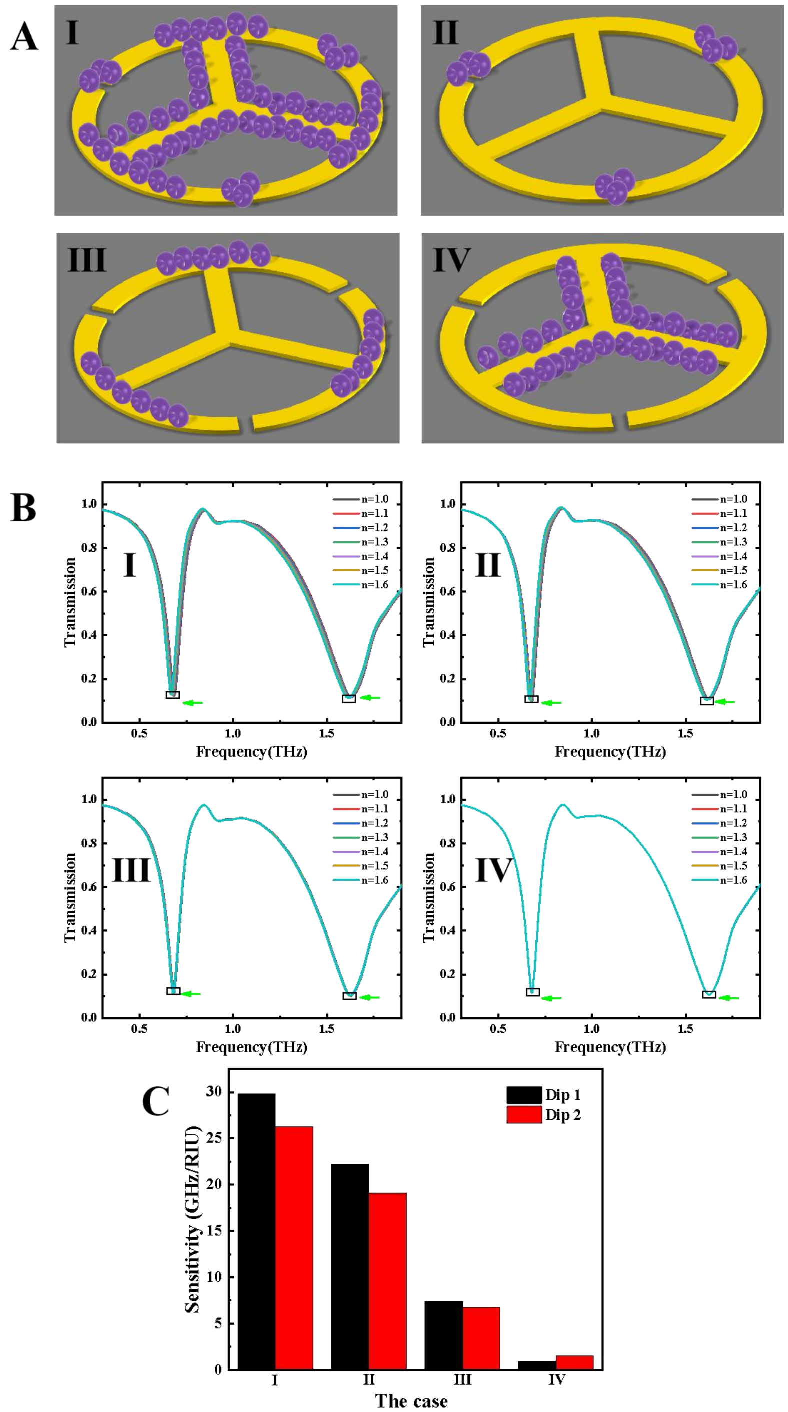

Figure S3 |(A)Four cases of analytes gathering on the surface of MMs.The simulated transmission spectra (B) and sensitivity (C) of the four cases, respectively.

Supplementary Figure S4

We have made a discussion of target samples with different quantities located promiscuously in different position. To further describe the inhomogeneous aggregation of analytes on the chip surface, the analytes are divided into four cases in a 2×2 array, as shown in **Figure S4**.

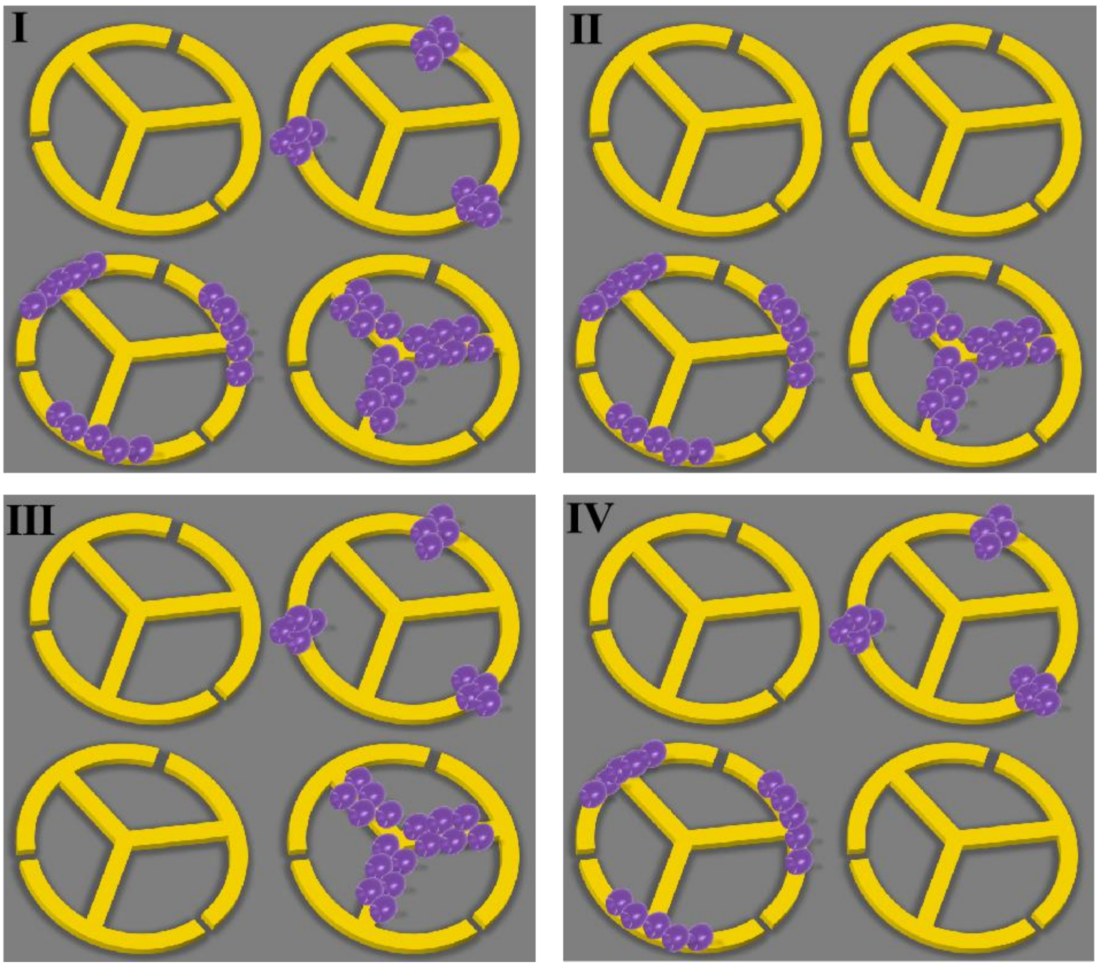

Figure S4 |Four cases of analytes gathering on the surface of MM sensors.

Supplementary Figure S5

Upon increasing n from 1.1 to 1.6, the transmission spectra under the four cases of the **Figure S4** are shown in **Figure S5A-D**. It can be seen that when the analyte gathers at the gap (I, III and IV in **Figure S4**), the similar frequency shift can be presented, which effectively confirmed the resonant properties of LC circuit and gap antennas are strongly determined by the field enhancement and the near-field coupling in the gap area and the proposed terahertz meta-biosensor has good stability.

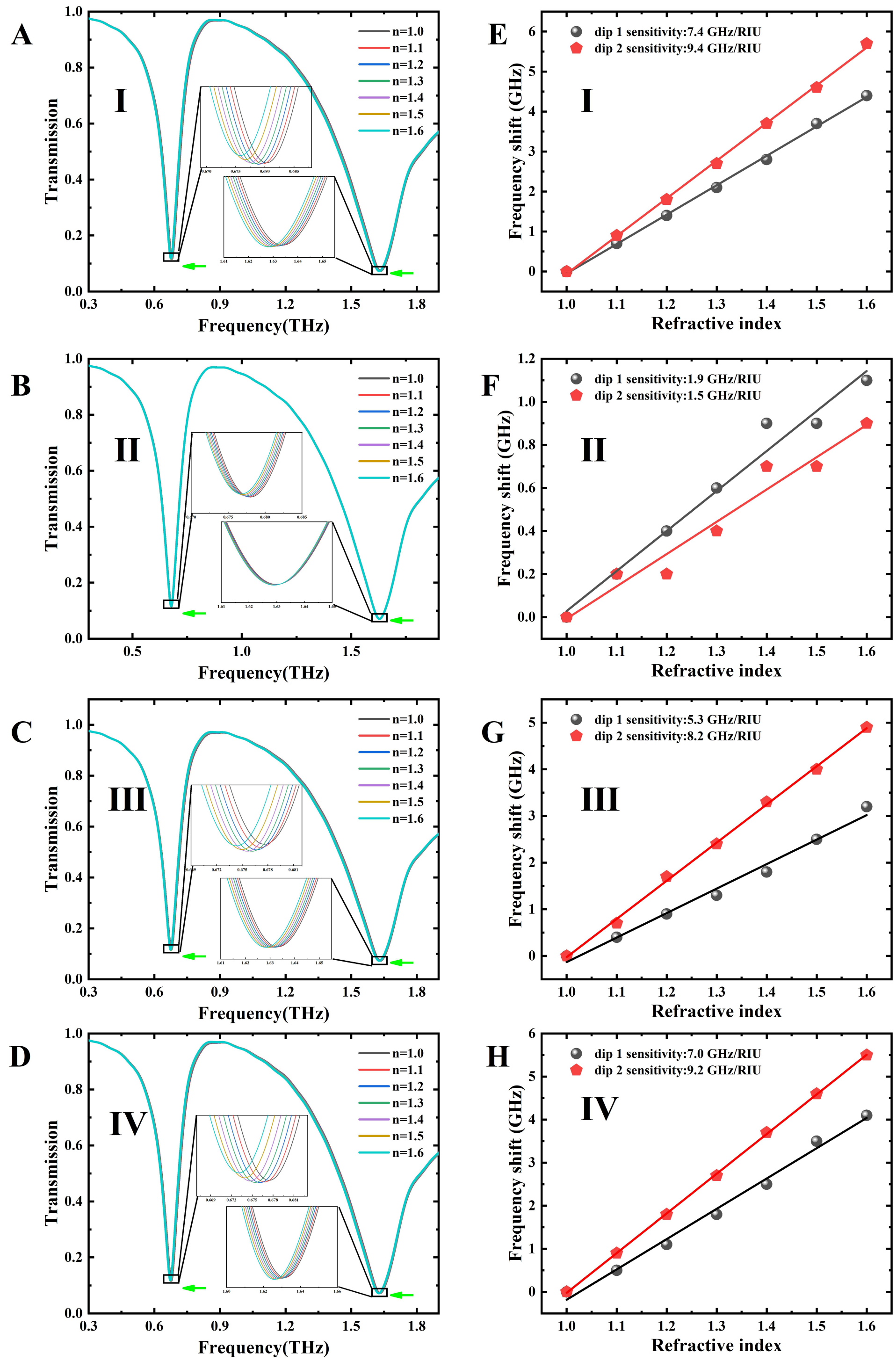

Figure S5 | (A-D) The transmission spectra of MM sensors for four cases under various refractive indices. (E-H) The corresponding relationship.